Journal of Power Sources 196 (2011) 855–859

Contents lists available at ScienceDirect

Journal of Power Sources

journal homepage: www.elsevier.com/locate/jpowsour

Short communication

Preparation and capacitive property of manganese oxide nanobelt bundles with birnessite-type structure

Xiuhua Tang[a,b], Hongjuan Li[a,b], Zong-Huai Liu[a,b,*], Zupei Yang[a,b], Zenglin Wang[a,b]

[a] Key Laboratory of Applied Surface and Colloid Chemistry, Shaanxi Normal University, Ministry of Education, Xi'an, 710062, PR China
[b] School of Chemistry and Materials Science, Shaanxi Normal University, Xi'an, 710062, PR China

ARTICLE INFO

Article history:
Received 13 April 2010
Received in revised form 23 May 2010
Accepted 21 June 2010
Available online 1 July 2010

Keywords:
Layered manganese oxide
Nanobelt bundle
Hydrothermal treatment
Capacitance

ABSTRACT

One-dimensional manganese oxide nanobelt bundles with layered structure have been synthesized by hydrothermally treating the precursor, K-type layered manganese oxide in a NaOH solution of 6.0 mol L^{-1} at 150 °C for 30 h. The obtained material is characterized by XRD, SEM, TEM and BET analysis. The manganese oxide nanobelt bundles are more than 50 μm long and 20–50 nm wide, and the specific surface area is about 160 m^2 g^{-1}. The electrochemical property of the synthesized manganese oxide nanobelt bundles has been studied using cyclic voltammetry in a mild aqueous electrolyte. The manganese oxide nanobelt bundle exhibits good capacitive behavior and cycling stability in a neutral electrolyte system, and its initial capacitance value is 268 F g^{-1}.

1. Introduction

Electrochemical supercapacitors show a promising application in energy storage devices [1,2]. There are two different type electrochemical capacitors based on their energy storage mechanisms, which are electrochemical double-layer capacitors based on carbon electrodes and pseudocapacitors with transition metal oxides and others as electrode materials [3–5]. Among the transition metal oxides, manganese oxide has been extensively studied; it can be used as good candidate electrode material because of its abundance, low-cost, good electrochemical reactivity and environmental friendliness in comparison with the ruthenium oxides or other transition metal oxides [6–8]. Up to now, many manganese oxides with various structures and morphologies have been fabricated via electrochemical and chemical routes, and their electrochemical properties have been investigated. The investigated materials mainly focus on the amorphous or poorly crystallized manganese oxides, and manganese oxide thin films [9–11]. The research results indicate that manganese dioxide have shown an average specific capacitance of 160 F g^{-1}, while the manganese dioxide thin films have a capacitance in the range between 100 and 400 F g^{-1} due to high utilization of the materials [12–14], which are far from its theoretical specific capacitance of ~1000 F g^{-1}. Therefore, manganese oxides with high specific capacitance, good cyclic stability and low fabrication cost are expected to be synthesized.

Research results show that the specific capacitance of the electrode materials is related to their specific surface area, the electrical conductivity in the solid phase and ionic transport within the pores [15]. In this regard, one-dimensional (1D) nanobelt materials not only give large electrode surface area and surface to volume ratio to contact with an electrolyte, which will provide conducting pathways for ions and electron and result in a high capacity and fast kinetics [16], but also provide better accommodation of large volume changes which results in improved cycle performance of the cathode materials [17]. Till now, 1D nanostructured manganese dioxide materials with different crystal structures have been fabricated by a sol–gel technology [6,18], electrochemical deposition technology [19], hydrothermal treatment methods [20] and so on. Ge et al. have prepared 1D ultralong layered K-birnessite bundles by a PEG-assisted hydrothermal method based on the reaction of $KMnO_4$ with 2-ethylhexanol, but γ-Mn_2O_3 as an impurity is detected [21]. Ma et al. have prepared 1D Na-birnessite nanobelts by a hydrothermal reaction in a 10 mol L^{-1} of NaOH solution using Mn_2O_3 as precursor, and they have found the obtained Na-birnessite nanobelts exhibit enhanced Li ions intercalation properties in comparison with the bulk manganese oxide [22]. Therefore, one-dimensional (1D) nanostructure materials with different morphology and large surface area are expected for potential applications in the electrochemical capacitor. In this work, manganese oxide nanobelt bundle with layered structure was prepared at 150 °C for 30 h by a simple method of hydrothermally treating K-type layered manganese oxide in a

* Corresponding author at: School of Chemistry and Materials Science of Shaanxi Normal University, 199 Changan South Road, Xi'an, Shaanxi 710062, China. Tel.: +86 29 85308442; fax: +86 29 85307774.
E-mail address: zhliu@snnu.edu.cn (Z.-H. Liu).

0378-7753/$ – see front matter © 2010 Elsevier B.V. All rights reserved.
doi:10.1016/j.jpowsour.2010.06.067

NaOH solution of 6.0 mol L^{-1}, and its electrochemical capacity was studied.

2. Experimental

2.1. Preparation of manganese oxide nanobelt bundles

The precursor, K-birnessite manganese oxide, was prepared by a sol–gel method as described in literature [23]. A $KMnO_4$ solution (0.38 mol L^{-1}, 50 mL) was added quickly to a glucose solution (1.4 mol L^{-1}, 20 mL) under vigorous stirring. The resulting mixture was further stirred for 10–15 s and then kept without further agitation, and a brown gel was obtained within 30 s of initial mixing. The brown gel was cooled at room temperature for 30 min, and then dried at 110 °C overnight, resulting in a brown xerogel. After the brown xerogel was calcined at 400 °C for 2 h, a fine gray powder was obtained. The powder was thoroughly washed with water and dried at 110 °C overnight, the precursor, K^+-type birnessite manganese oxide was obtained, which was abbreviated as K-BirMO.

The precursor, K-BirMO (0.6 g) was added in NaOH solution (6.0 mol L^{-1}, 36 mL) under vigorous stirring to form a homogenous suspension, and then the homogenous suspension was transferred into a Teflon-lined stainless steel autoclave with a capacity of 50 mL. The autoclave was maintained at 150 °C for 30 h and then cooled to room temperature naturally. The resultant product was collected by filtration, washed several times with distilled water, and dried at 50 °C overnight. Manganese oxide nanobelt bundle with layered structure was finally prepared, which was abbreviated as BirMO nanobelt.

2.2. Characterization

The powder X-ray diffraction pattern was recorded on a D/Max-3c X-ray diffractometer with Cu-Kα (λ = 1.5406 Å), using an operation voltage and current of 40 kV and 40 mA, respectively. SEM images were taken using a Quanta 200 environmental scanning electron microscopy operated at the accelerating voltage of 20 kV. Transmission electron microscopy (TEM) and high-resolution TEM (HR-TEM) characterization were performed with a JEM-3010 transmission electron microscope (CCD, Gatan894). Specimens for TEM observation were prepared by dispersing the manganese oxide powder into alcohol by an ultrasonic treatment. A Beckman coulter-type nitrogen adsorption–desorption apparatus (ASAP 2020M) was used to investigate the pore property degassing for 4 h below 10^{-3} mm Hg. A CHI 600 electrochemical workstation (Chenhua Instrument Co., Shanghai, China) was used for electrochemical measurements.

2.2.1. Electrochemical measurement

Electrodes were prepared by mixing the obtained materials (80 wt.%) as active material with acetylene black (15 wt.%) and polyvinylidene fluoride (5 wt.%). The first two constituents were firstly mixed together to obtain a homogeneous black powder. The polyvinylidene fluoride solution (0.02 g mL^{-1}, in *N*-methylketopyrrolidine) was then added. This resulted in a rubber-like paste, which was brush-coated onto a Ni mesh. The mesh was dried at 110 °C in air for 2 h for the removal of the solvent. After drying, the coated mesh was uniaxially pressed to completely adhere to the electrode material with the current collector.

A beaker type electrochemical cell was equipped with the obtained material as a working electrode, a Pt-foil (2 cm^2) as the counter electrode and saturated calomel electrode (SCE) as the reference electrode. CV curves were taken between −0.2 and 0.8 V in a Na_2SO_4 electrolyte (1.0 mol L^{-1}) at a sweep rate of 5 mV s^{-1}. The average specific capacitance was evaluated from the area of the charge and discharge curves of the CV plot according to the following equation [24]:

$$C_m = \frac{i}{mv}$$

where m is the total mass of active materials in the electrode, v is the potential sweep rate, and i is the even current response, which is obtained through integrating the area of the curve.

3. Results and discussion

3.1. Crystalline structure and morphology

The precursor, K-BirMO shows a layered structure characteristic, and its basal spacing is 0.71 nm (Fig. 1a). After K-BirMO is treated in a NaOH solution at 150 °C for 30 h, the layered structure still maintains and the basal spacing hardly changes, and only the peak intensity increases for the obtained BirMO nanobelt (Fig. 1b). The lattice constants of sample BirMO nanobelt are calculated to be a = 2.85 Å and c = 21.57 Å, which are essentially identical with those reported for potassium manganese oxide hydrate $K_xMnO_2{\cdot}yH_2O$ (JCPDS 52-0556). These results indicate that the layered structure can be maintained when K-BirMO is hydrothermally treated in a NaOH solution at 150 °C for 30 h.

SEM image of K-BirMO shows an irregular plate-like morphology (Fig. 2a), while sample BirMO nanobelt is dominated by the very long flexible bundles assembled with nanobelts (Fig. 2b). The manganese oxide nanobelt bundles are usually more than 50 μm long and 20–50 nm wide. SEM images suggest that the hydrothermal treatment of the precursor, K-BirMO in NaOH solution causes an obvious morphology change although no crystalline structure changes. TEM image of sample BirMO nanobelt clearly shows that the bundles are assembled with thick nanobelts along the belt axis direction (Fig. 2c). HR-TEM image of the nanobelt bundles obtained from Fig. 2c (indicated by the black pane) shows an interplanar spacing of about 0.56 nm (Fig. 2d). The width of 0.56 nm and 0.24 nm from neighboring fringes of an individual nanobelt corresponds to the (0 0 2) and (1 0 1) planes of manganese oxide nanobelt bundles, respectively. In general, H-type layered manganese oxide contains one molecular layer of water between the manganese oxide sheets. Because the thickness of the manganese

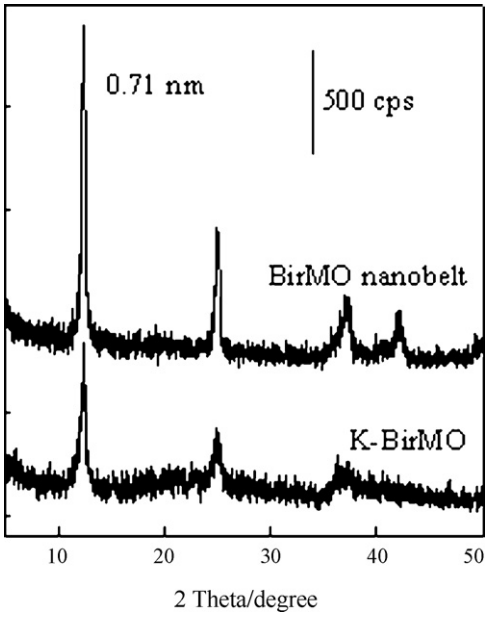

Fig. 1. XRD patterns of samples K-BirMO and BirMO nanobelt.

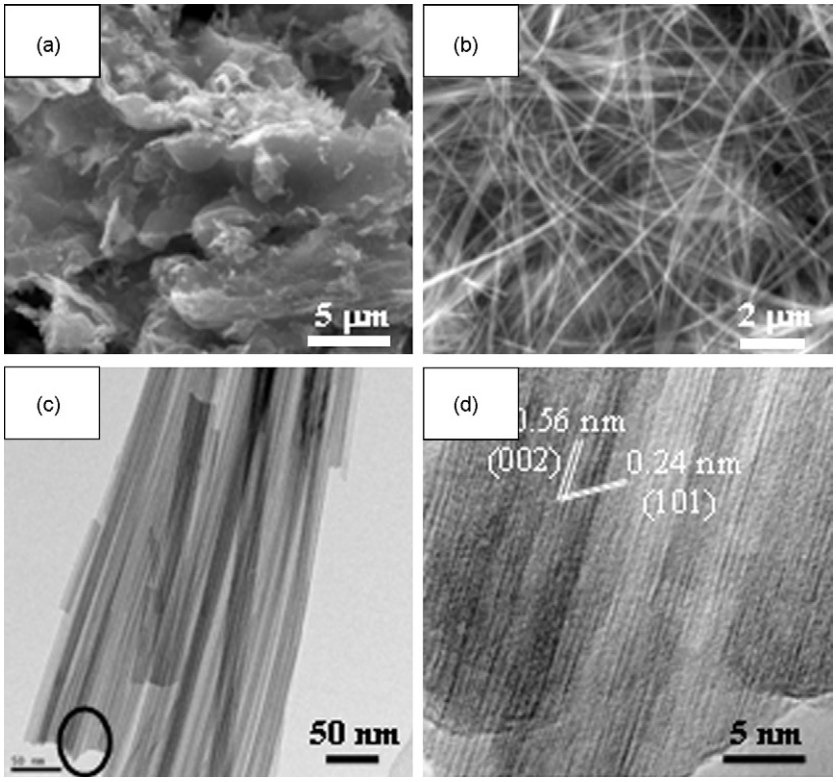

Fig. 2. SEM image of sample K-BirMO (a), SEM (b), TEM (c) and HR-TEM (c) images of sample BirMO nanobelt.

oxide layer is 0.45 nm and the diameter of water molecules is about 0.28 nm [25,26], the H-type layered manganese oxide has a basal spacing of about 0.73 nm. In sample BirMO nanobelt, additional water layers do not form, and therefore K^+ ions may be randomly exchanged with the monolayer water molecules, producing a structure similar to that of synthetic potassium birnessite. When the water molecules are radiated by high energy electron beam during the TEM experiment, the electron beam radiation causes a removal of the water molecules from the interlayer of the layered birnessite, which results in an interplanar space shrinkage and gives a new layered manganese oxide phase with an interplanar spacing of about 0.56 nm with only K^+ ions existing between manganese oxide layers (JCPDS 27-0751) [27].

3.2. Surface area

N_2 adsorption–desorption isotherms of the precursor, K-BirMO in comparison with BirMO nanobelts synthesized in a NaOH solution of 6.0 mol L^{-1} at 150 °C for 30 h are shown in Fig. 3. The precursor, K-BirMO is apparently non-porous, having a Brunauer–Emmett–Teller (BET) surface area of 38 m^2 g^{-1} (Fig. 3, bottom). In contrast, the isotherm feature of the sample BirMO nanobelts clearly indicates the presence of mesopores in this sample, classified as type IV as defined by the International Union of Pure and Applied Chemistry (IUPAC) (Fig. 3, above) [28]. A hysteretic loop between the adsorption and desorption branches can be considered as type H3, indicative of slit-like pores. Sample BirMO nanobelts show a much higher BET surface area of 160 m^2 g^{-1} and larger N_2 adsorption volume. The BET surface area is larger than that reported by Wei et al. [29], in which nanostructured MnO_2 is obtained and its BET surface area is of 132 m^2 g^{-1}. A *t*-plot analysis and BJH average pore diameter of 15.4 nm confirm the predominant presence of mesopores in sample BirMO nanobelts. The mesoporous surface area is about 142 m^2 g^{-1}, and contributed to about 89% of the total specific surface area. These results clearly indicate that the formation of the nanobelt bundles in sample BirMO nanobelts drastically enhances the mesoporosity as well as the specific surface area.

3.3. Electrochemical property

Extensive studies have shown that manganese oxides are promising electrode materials for electrochemical supercapacitors, while cyclic voltammetry is an important tool to investigate the capacitive behavior of the obtained materials. Fig. 4 shows the first cyclic voltammetry curves of the K-BirMO and BirMO nanobelt electrodes. The CV curves of two samples obtained in a Na_2SO_4 (1.0 mol L^{-1}) solution at a sweep rate of 5 mV s^{-1} shows relatively rectangular mirror images with respect to the zero-current line,

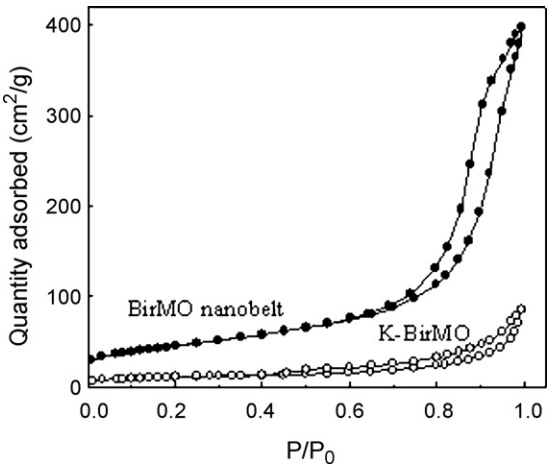

Fig. 3. N_2 adsorption–desorption isotherms of samples K-BirMO and BirMO nanobelt.

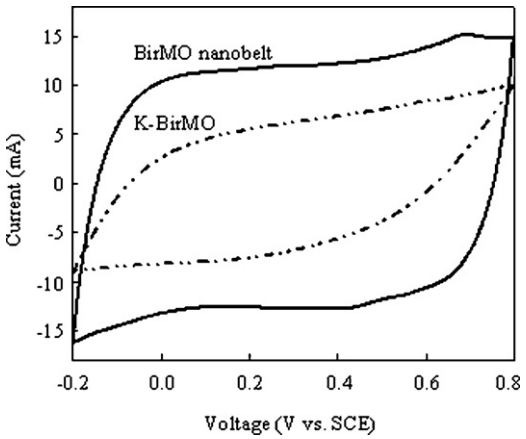

Fig. 4. The first CV curves of samples K-BirMO and BirMO nanobelt at a scan rate of 5 mV s^{-1} in 1 M Na_2SO_4 solution.

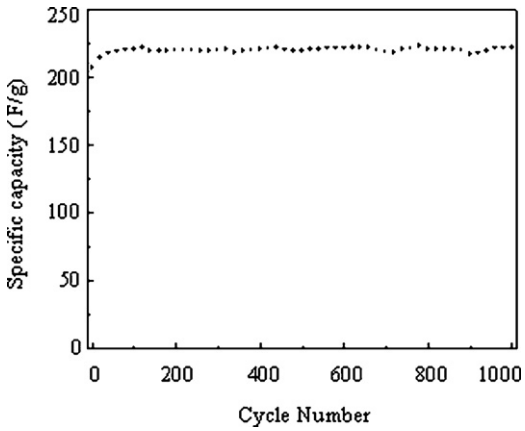

Fig. 6. The variation of specific capacitance of sample BirMO nanobelt over 1000 cycles at 10 mV s^{-1}.

indicating a obvious capacitive behavior for the obtained materials. Meanwhile, these curves show no peaks in the range between −0.2 and 0.8 V, indicating that the electrode capacitor is charged and discharged at a pseudoconstant rate over the complete voltammetric cycle [7,30]. The CV curve of the K-BirMO electrode is distorted, while the one of the electrode obtained from sample BirMO nanobelts exhibits good symmetrical characteristics, suggesting that the reversibility of the K-BirMO electrode is not good at this potential range. For sample BirMO nanobelts, the specific capacitance value calculated from the cyclic voltammetry curve is found to be 268 F g^{-1}, indicating the BirMO nanobelts prepared by the present method behave as good capacitor within the window of −0.2 to 0.8 V. The good electrochemical behavior may be ascribed to the relative large amount of manganese and large BET surface area. Electrochemical property of sample BirMO nanobelt is more elucidated by CV cyclic voltammetry in a 1 M Na_2SO_4 solution in the range between −0.2 and 0.8 V at different potential scan rates ranging from 2 to 30 mV s^{-1} (Fig. 5). At lower scan rates, the rectangular characteristic of CV curves hardly changes, indicating almost ideal good capacitive behavior for the obtained materials (Fig. 5 a–d). Even if at relative high scan rate of 30 mV s^{-1}, the relatively rectangular mirror image with respect to the zero-current line is also found (Fig. 5e), indicating that sample BirMO nanobelts show a high reaction activity and reversibility.

The cycle performances are of important for the supercapacitor. The long-term stability of sample BirMO nanobelt based on as-prepared powder upon cycling is investigated and the variation of specific capacitance over 1000 cycles at 10 mV s^{-1} is depicted in Fig. 6. A capacitance increase behavior is observed upon cycling and the capacitance increase remains stable and close to 222 F g^{-1} after 1000 cycles. Similar improvement of the specific capacitance upon cycling has also been reported for MnO_2 thin films [31] and α-MnO_2 [7]. The specific capacitance increase is probably attributed to the increase of the active points due to the incomplete intercalation or de-intercalation of the guest ions at relative high scan rate. The electrode can withstand 1000 cycles without significant capacitance loss. This demonstrates that, within the test voltage window, the intercalation and de-intercalation processes of the guest ions do not seem to induce significant structural or meso-structural changes of the electrode as expected for pseudocapacitive reactions. In comparison with the first curve, the shape of the 1000th curve of sample BirMO nanobelt at 10 mV s^{-1} is more like a rectangle (Supporting information Figure S1, left), and the nanobelt morphology is still maintained (Fig. S1, right), indicating that sample BirMO nanobelt shows a relatively good cycling stability.

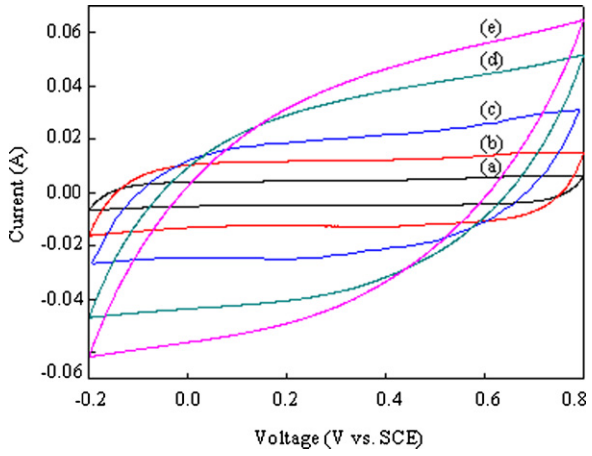

Fig. 5. CV curves of sample BirMO nanobelt in a 1 M Na_2SO_4 solution at different potential scan rates ranging from 2 to 30 mV s^{-1}, respectively: (a) 2 mV s^{-1}, (b) 5 mV s^{-1}, (c) 10 mV s^{-1}, (d) 20 mV s^{-1}, and (e) 30 mV s^{-1}.

Until now, two mechanisms have been proposed to explain the MnO_2 charge storage behavior. The firstly mechanism is based on the concept of intercalation of H^+ or alkali metal cations such as Na^+ ions in the electrode during reduction and de-intercalation upon oxidation.

$$MnO_2 + A + e^- \leftrightarrow MnOOA$$

And the secondary one is based on the surface adsorption of electrolyte cations.

$$(MnO_2)_{surface} + A + e^- \leftrightarrow (MnO_2{}^-A)_{surface}$$

In the present study, we think that the redox process is mainly governed by the intercalation and de-intercalation of Na^+ ions from the electrolyte into the mesoporous manganese oxide nanobelt, similar to the work reported by Toupin et al. [32].

4. Conclusion

One-dimensional manganese oxide nanobelt bundles with layered structure have been synthesized by hydrothermally treating the precursor, K-BirMO, in a solution of 6.0 mol L^{-1} NaOH at 150 °C for 30 h. The as-prepared manganese oxide nanobelt bundles not only have a large area of 160 m^2 g^{-1}, but also show good capacitive behavior and cycling stability in a neutral electrolyte system. The specific capacitance of sample BirMO nanobelt is 268 F g^{-1}, and also shows a good cycling stability.

Supporting information

The first and the 1000th CV curves of sample BirMO nanobelt at a scan rate of 10 mV s^{-1} in 1 mol L^{-1} Na_2SO_4 solution (above) and TEM image of the obtained material after the 1000th cycling (bottom). These materials are available free of charge via the Internet at http://www.sciencedirect.com.

Acknowledgements

We thank National High Technology Research and Development Program of China (2007AA03Z248) and National Natural Science Foundation of China (20971082) for financial support of this research.

Appendix A. Supplementary data

Supplementary data associated with this article can be found, in the online version, at doi:10.1016/j.jpowsour.2010.06.067.

References

[1] B.E. Conway, Electrochemical Supercapacitors, Kluwer Academic/Plenum Publishers, New York, 1999.
[2] D. Liu, B.B. Garcia, Q. Zhang, Q. Guo, Y. Zhang, S. Sepehri, G. Cao, Adv. Mater. 19 (2009) 1015–1023.
[3] C. Arbizzani, M. Mastragostino, F. Soavi, J. Power Sources 100 (2001) 164–170.
[4] T.-Y. Wei, C.-H. Chen, H.-C. Chien, S.-Y Lu, C.-C. Hu, Adv. Mater. 22 (2010) 347–351.
[5] H. Zhang, G. Cao, Z. Wang, Y. Yang, Z. Shi, Z. Gu, Nano. Lett. 8 (2008) 2664–2668.
[6] X.Y. Wang, W.G. Huang, P.J. Sebastian, S. Gamboa, J. Power Sources 140 (2005) 211–215.
[7] M. Toupin, T. Brousse, D. Bélanger, Chem. Mater. 14 (2002) 3946–3952.
[8] L. Athouēl, F. Moser, R. Dugas, O. Crosnier, D. Bélanger, T. Brousse, J. Phys. Chem. C 112 (2008) 7270–7277.
[9] C.J. Xu, B.H. Li, H.D. Du, F.Y. Kang, Y.Q. Zeng, J. Power Sources 180 (2008) 664–670.
[10] S.L. Chou, F.Y. Cheng, J. Chen, J. Power Sources 162 (2006) 727–734.
[11] B. Dong, T. Xue, C.L. Xu, H.L. Li, Micropor. Mesopor. Mater. 112 (2008) 627–631.
[12] C.K. Lin, K.-H. Chuang, C.-Y. Lin, C.Y. Tsay, C.-Y. Chen, Surf. Coat. Technol. 202 (2007) 1272–1276.
[13] M. Nakayama, A. Tanaka, Y. Sato, T. Tonosaki, K. Ogura, Langmuir 21 (2005) 5907–5913.
[14] K.-W. Nam, M.G. Kim, K.-B. Kim, J. Phys. Chem. C 111 (2007) 749–758.
[15] J.Y. Luo, L. Cheng, Y.Y. Xia, Electrochem. Commun. 9 (2007) 1404–1409.
[16] F. Cheng, J. Zhao, W. Song, C. Li, H. Ma, J. Chen, P. Shen, Inorg. Chem. 45 (2006) 2038–2044.
[17] J.-H. Kim, T. Ayalasomayajula, V. Gona, D. Choi, J. Power Sources 183 (2008) 366–369.
[18] J. Liu, Y.-C. Son, J. Cai, X. Shen, S.L. Suib, M. Aindow, Chem. Mater. 16 (2004) 276–285.
[19] M.-S. Wu, P.-C. Julia Chiang, J.-T. Lee, J.-C. Lin, J. Phys. Chem. B 109 (2005) 23279–23284.
[20] J. Chen, X. Tang, J. Liu, E. Zhan, J. Li, X. Huang, W. Shen, Chem. Mater. 19 (2007) 4292–4299.
[21] J. Ge, L. Zhuo, F. Yang, B. Tang, L. Wu, C. Tung, J. Phys. Chem. B 110 (2006) 17854–17859.
[22] R. Ma, Y. Bando, L. Zhang, T. Sasaki, Adv. Mater. 16 (2004) 918–991.
[23] S. Ching, D.J. Petrovay, M.L. Jorgensen, Inorg. Chem. 36 (1997) 883–890.
[24] C.Z. Yuan, B. Gao, X.G. Zhang, J. Power Sources 173 (2007) 606–612.
[25] J.E. Post, D.R. Veblen, Am. Mineral. 75 (1990) 477–489.
[26] Z.-H. Liu, K. Ooi, H. Kanoh, W. Tang, T. Tomida, Langmuir 16 (2000) 4154–4164.
[27] A. Eftekhari, M. Kazemzad, F. Moztarzadeh, Mater. Res. Bull. 40 (2005) 2205–2211.
[28] L. Wang, K. Takada, A. Kajiyama, M. Onoda, Y. Michiue, L. Zhang, M. Watanabe, T. Sasaki, Chem. Mater. 15 (2003) 4508–4514.
[29] V. Subramanian, H.W. Zhu, B.Q. Wei, J. Power Sources 159 (2006) 361–364.
[30] X. Zhang, W. Yang, D.G. Evans, J. Power Sources 184 (2008), 695-670.
[31] S.C. Pang, M.A. Anderson, T.W. Chapman, J. Electrochem. Soc. 147 (2000) 444–450.
[32] M. Toupin, T. Brousse, D. Bélanger, Chem. Mater. 16 (2004) 3184–3190.